Journal of Asian Earth Sciences 154 (2018) 342–353

Contents lists available at ScienceDirect

Journal of Asian Earth Sciences

journal homepage: www.elsevier.com/locate/jseaes

Full length article

Constraints of texture and composition of clinopyroxene phenocrysts of Holocene volcanic rocks on a magmatic plumbing system beneath Tengchong, SW China

Jun-Hao Hu[a,b], Xie-Yan Song[a,*], Hai-Long He[a,b], Wen-Qin Zheng[a], Song-Yue Yu[a], Lie-Meng Chen[a], Chun-Kit Lai[c,d]

[a] State Key Laboratory of Ore Deposit Geochemistry, Institute of Geochemistry, Chinese Academy of Sciences, Guiyang 550081, PR China
[b] University of Chinese Academy of Sciences, Beijing 100049, PR China
[c] Faculty of Science, Universiti Brunei Darussalam, Gadong BE1410, Brunei Darussalam
[d] ARC Centre of Excellence in Ore Deposits (CODES), University of Tasmania, Hobart, Tasmania 7001, Australia

ARTICLE INFO

Keywords:
Tengchong (Yunnan, SW China)
Clinopyroxene phenocryst
Holocene volcanoes
Magma chamber
Thermobarometric calculations

ABSTRACT

Understanding processes of magma replenishment in a magma plumbing system is essential to predict eruption potential of a dormant volcano. In this study, we present new petrologic and thermobarometric data for youngest lava flows from the Holocene Heikongshan volcano in the Tengchong area, SW China. Clinopyroxene phenocrysts from the trachytic lava flows display various textural/compositional zoning styles (i.e., normal, reverse and oscillatory). Such zoning patterns are indicative of an open magmatic plumbing system with multiphase magma replenishment and mixing, which were likely a key drive of the volcanic eruptions. Thermobarometric calculations of these zoned clinopyroxene phenocrysts yield crystallization pressures of 3.8–7.1 kbar (peak at 4.5–7.0 kbar), corresponding to a magma chamber at depths of 14–21 km. The calculated depths are consistent with the large low-resistivity body at 12–30 km beneath the Heikongshan volcano, implying that the magmatic plumbing system may still be active. Recent earthquakes in the Tengchong area suggest that the regional strike-slip faulting are still active, and may trigger future volcanic eruptions if the magma chamber(s) beneath the Tengchong volcanic field is disturbed, in spite of the volcanic quiescence since 1609 CE.

1. Introduction

Phenocrysts are the minerals that crystallized in magma chambers before volcanic eruptions occur, and hence textural/compositional zoning of phenocrysts can preserve useful information on physico-chemical conditions (e.g., pressure and temperature) and magmatic processes (e.g., fractionation and magma mixing) of the magma chambers (Hibbard, 1981; Anderson, 1984; Tepley et al., 2000; Morgan and Blake, 2006; Humphreys et al., 2006; Ginibre et al., 2007; Kahl et al., 2011). Such information, integrated with geophysical data, is invaluable to understand the key factors that trigger volcanic eruptions (Gerbe and Thouret, 2004; Samaniego et al., 2011; Rivera et al., 2014), and has successfully forecasted the eruptions of many active volcanoes, e.g., Tarumai volcano (Japan) (Gerbe and Thouret, 2004; Nakagawa et al., 2011; Dahren et al., 2012; Longpre et al., 2014).

Cenozoic volcanoes extend from the SE Tibetan Plateau, through the Tengchong area in Yunnan to central-western Myanmar and form a volcanic belt. Notably Mt Popa in Myanmar and Heikongshan volcano in Yunnan (Fig. 1a and b). In the Tengchong area, many volcanoes are considered dormant/extinct because there is no volcanic eruption since 1609 CE (late Ming Dynasty) (Liu, 1999). Nevertheless, a recent discovery of low-velocity and low-resistivity bodies (10–30 km deep) by magnetotelluric and seismic tomographic surveys (Wang and Huangfu, 2004; Jiang et al., 2012; Xu et al., 2012; Yang et al., 2013; Wu et al., 2016) has raised concerns over potential future volcanic eruptions in this populated and famous tourist destination in SW China. In this paper, therefore, we present a comprehensive study of the magmatic processes beneath these dormant volcanoes, and predict the likelihood of future volcanic eruptions in the Tengchong area.

The Heikongshan volcano is one of the major dormant Cenozoic volcanoes in the Tengchong area (Fig. 1b). The region around this volcano is characterized by high geothermal gradient and $^{3}He/^{4}He$ ratios, which suggest constant mantle-derived input (Zhao et al., 2012). In this study, we have sampled the two youngest lava flows of the

* Corresponding author at: State Key Laboratory of Ore Deposit Geochemistry, Institute of Geochemistry, Chinese Academy of Sciences, 99 Lincheng West Road, Guanshanhu District, Guiyang 550081, PR China.
E-mail address: songxieyan@vip.gyig.ac.cn (X.-Y. Song).

https://doi.org/10.1016/j.jseaes.2017.12.029
Received 1 September 2017; Received in revised form 19 December 2017; Accepted 24 December 2017
Available online 02 January 2018
1367-9120/

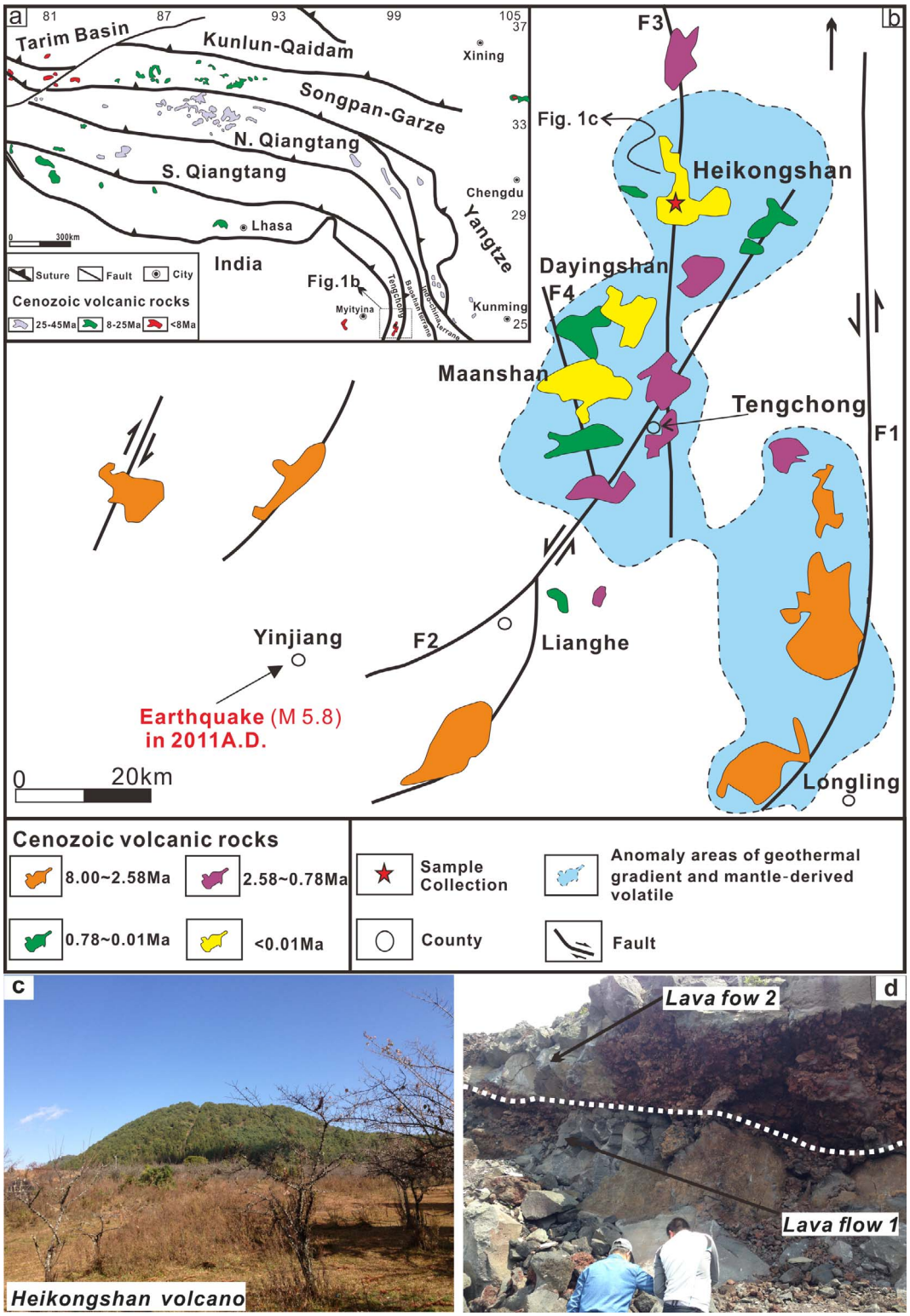

Fig. 1. (a) Distribution of Cenozoic volcanic rocks in the Tibetan plateau and adjacent areas (modified from Mo et al. (2006)). (b) Geological map showing the distribution of Cenozoic volcanic rocks in Tengchong area (modified from Li et al. (2000); Wang et al. (2007); Zhou et al. (2012); Guo et al. (2015)). Abbreviations: F1, Longchuanjiang fault; F2, Dayingjiang fault; F3, Longchuan fault; F4, Xinqi fault. (c) Landscape of the Heikongshan volcano. (d) Field relationships between the two lava flows of the Heikongshan volcano.

Heikongshan volcano. We suggest that the textural/compositional zoning (reverse and oscillatory) of the clinopyroxene phenocrysts is indicative of multiphase magma replenishment and mixing inside magma chamber(s), which built up magmatic stress and eventually led to volcanic eruptions.

2. Geological setting

Cenozoic volcanic rocks in the Tibetan Plateau are mainly distributed along the Qiangtang (ca. 45–25 Ma) and Songpan-Garze belts (ca. 25–8 Ma) (Fig. 1a; Mo et al., 2006). These Cenozoic volcanic rocks are dominantly potassic/shoshonitic and were formed under post-collisional

(India-Asia collision) tectonics (i.e., the Himalayan Orogeny; Yin and Harrison, 2000; Chung et al., 2005; Mo et al., 2006; Zhao et al., 2009). The Quaternary volcanic rocks are spatially confined to the NW-, NE- and SE-margins of the Tibetan Plateau (Fig. 1a). The Quaternary volcanoes in the Tengchong area (SE-margin of the Tibetan Plateau) are important from the volcanic hazard perspective: not only because of the large resident/tourist population in the area, but also because the active E-dipping subduction (India plate beneath the Burma–Tengchong terrane) has generated medium-large earthquakes that can trigger volcanic eruptions (Li et al., 2008; Lei et al., 2009, 2012a; He et al., 2010; Zhao et al., 2011).

Cenozoic volcanoes in the Tengchong area are situated between the Gaoligong and Nabang regional strike-slip faulting (Wang et al., 2007; Huang et al., 2013; Xu et al., 2015), with the volcanism occurred from the late Miocene (ca. 8 Ma) (Zhu et al., 1983; Kornfeld et al., 2014; Guo et al., 2015) to Quaternary (ca. 7 ka) (Nakai et al., 1993; Li et al., 2000; Yin and Li, 2000; Zou et al., 2010; Tucker et al., 2013). Most researchers agreed that the Tengchong volcanic rocks were generated by partial melting of the metasomatized mantle modified by subducted oceanic/continental materials (Zhu et al., 1983; Wang et al., 2006; Zou et al., 2014, 2017; Guo et al., 2015). The magma generation and eruption were likely linked to the regional strike-slip faulting (Wang and Huangfu, 2004; Wang et al., 2007; Lei et al., 2009; Zhou et al., 2012; Sun et al., 2016), as the Cenozoic volcanic rocks are mainly distributed along the N-S and NNE-trending faults (Fig. 1b). The Cenozoic volcanic rocks unconformably overlie the Paleozoic-Mesozoic sedimentary rocks and the Mesozoic–Cenozoic granites (Huangfu and Jiang, 2000). Based on stratigraphic and geochronological studies (^{30}Th–^{238}U, K/Ar and thermoluminescence), the Cenozoic volcanic rocks were erupted in four phases (Wang et al., 1999; Li and Liu, 2012; Zou et al., 2017): (1) late Miocene to Pliocene (ca. 8.00–2.58 Ma) olivine trachybasalt and minor basaltic trachyandesite, (2) early Pleistocene (ca. 2.58–0.78 Ma) dacite, (3) late Pleistocene (ca. 0.78–0.01 Ma) basaltic trachyandesite, and (4) Holocene (< 0.01 Ma) trachyandesite, trachyte and minor olivine basalt.

The Heikongshan volcano is located to the north of Tengchong city, and its volcanic cone morphology (lava cone with scoria cover) is well preserved (Fig. 1c). This volcano is about 250 m in diameter and 150 m tall, and the lava flowed out from the crater along the western, northern and eastern flanks of the volcano. The Heikongshan volcano erupted intermittently since the middle Pleistocene, and the latest eruption was K-Ar dated to be Holocene (ca. 7 ka; Nakai et al., 1993). The lava flows show a compositional evolution trend from basaltic trachyandesite to trachyte (Fig. 2a; Yu et al., 2012), similar to the nearby Holocene Mananshan and Dayingshan volcanoes (Zou et al., 2017; Fig. 2).

3. Sample descriptions

In this study, four samples were collected from the two youngest lava flows of the Heikongshan volcano. Older lava flows were not sampled because of the lack of outcrops. The youngest lava flows (termed lava flow 2 hereafter) are about 1.5 m, blocky and mildly vesicular. The older lava flow 1 is more vesicular than lava flow 2, and is not completely exposed (Fig. 1d). Two trachyandesite samples (TC14-6 and TC14-13) were collected from lava flow 1, and two trachyte samples (TC14-1 and TC14-18) were collected from lava flow 2. Microscopic petrography indicates that the volcanic rocks are moderately porphyritic with different amounts of phenocrysts. The four samples show similar phenocryst assemblage of plagioclase + clinopyroxene + orthopyroxene. Phenocrysts (7%) of the trachyandesite include 3% clinopyroxene, 2% orthopyroxene and 2% plagioclase, whereas phenocrysts (15%) of the trachyte include 8% plagioclase, 5% clinopyroxene and 1% orthopyroxene. Groundmass of the trachyandesite and trachyte is mainly composed of clinopyroxene, orthopyroxene and plagioclase with sparse Fe–Ti oxides.

The clinopyroxene phenocrysts in lava flow 1 are 0.5–1.2 mm in size and occur mainly as isolated crystals. They are euhedral to subhedral and predominantly granular. These clinopyroxene phenocrysts show three zoning patterns (i.e., reverse, oscillatory and normal) based on BSE (backscattered electron) images. The reverse zoning has a large core (about 500 μm) and a narrow rim (20–50 μm), with a jagged contact surface in between (Fig. 4a). The oscillatory zoning comprises a core, a mantle and a rim (of different size/thickness), with also jagged contact surface among them (Fig. 4c). The normal zoning is characterized by the absence of distinct resorption texture, which is common in the reverse and oscillatory zoning (Fig. 4a, c, and e).

Orthopyroxene phenocrysts from the trachyandesite (lava flow 1) are euhedral to subhedral and only show normal zoning (Fig. 4f), whilst the plagioclase phenocrysts in lava flow 1 are mainly euhedral to subhedral (Fig. 4i). The rim (ca. 100 μm) of the reversely-zoned clinopyroxene from lava flow 2 is thicker than its lava flow 1 counterparts (Figs. 4a–b and 5), and the degree of core-rim resorption of the former is also higher than that of the latter (Figs. 4a–b and 5). Similar textural features are also found in the oscillatory-zoned clinopyroxene from the two lava flows (Figs. 4c–d and 6). The textural and compositional zonings of the clinopyroxene phenocrysts from the lava flow 2 are well revealed through the EMPA elemental mapping (Figs. 5 and 6). The orthopyroxene phenocrysts in lava flow 2 show both normal and oscillatory zoning (Fig. 4g and h). Textures of the oscillatory-zoned orthopyroxene are similar to the oscillatory-zoned clinopyroxene (Fig. 4c

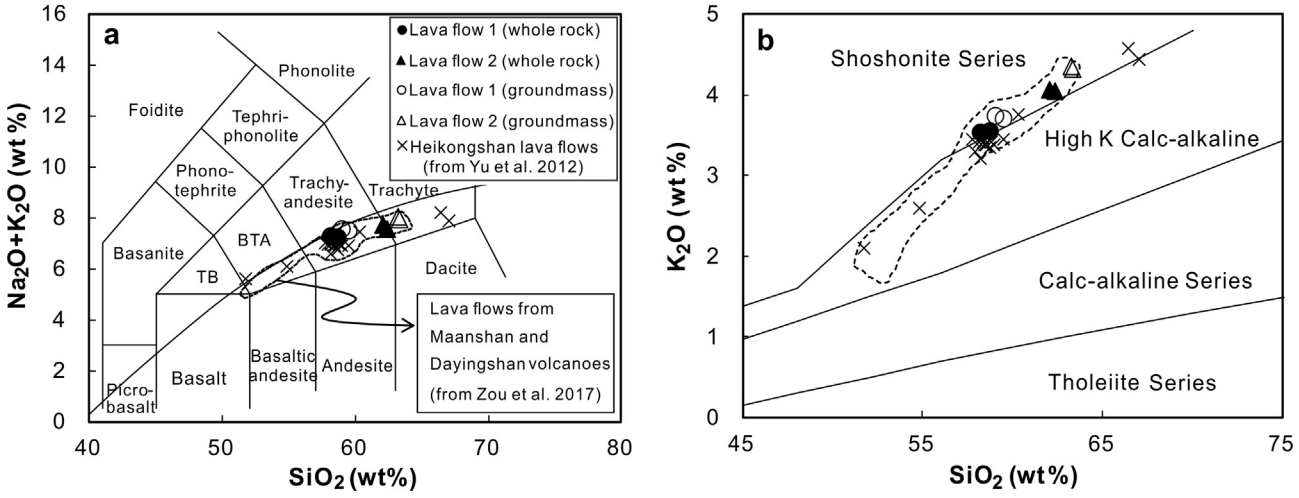

Fig. 2. (a) Total alkali ($Na_2O + K_2O$) vs. SiO_2 (TAS) diagram (after Le Maitre et al. (1989)) for the bulk rock and groundmass compositions of the Heikongshan lava flows. (b) K_2O vs. SiO_2. Abbreviations: TB = trachybasalt, BTA = basaltic trachyande.

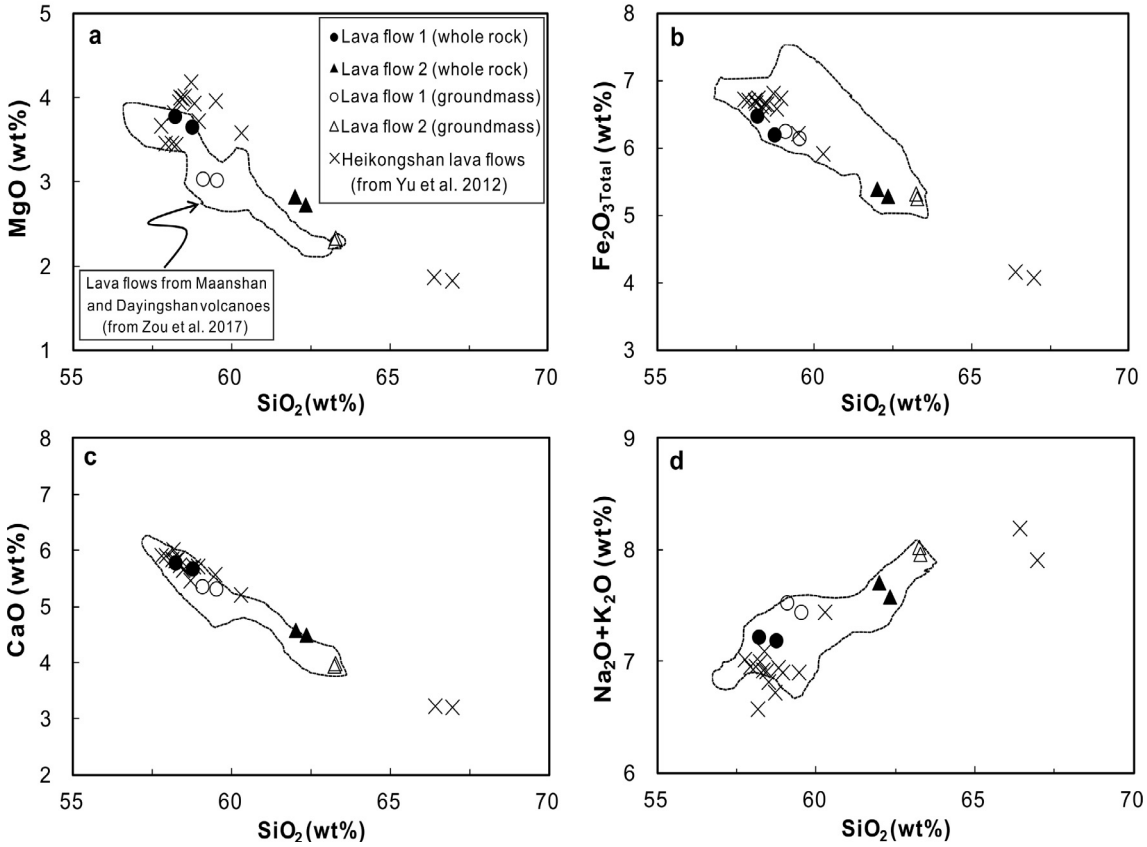

Fig. 3. Harker diagrams of SiO_2 vs. MgO, Fe_2O_{3Total}, CaO, $Na_2O + K_2O$ for the two lava flows of the Heikongshan volcano.

and d, h). Plagioclase phenocrysts from lava flow 2 also occur as oikocryst enveloping the pyroxene grains (Fig. 4j).

4. Analytical methods

Determination of the equilibrium melt compositions is necessary for accurate P-T calculation using clinopyroxene-melt thermobarometry. Therefore, the groundmass of the four Heikongshan volcanic rock samples was separated to represent the melt equilibrated with the phenocrysts. Firstly, 2–3 kg of the fresh rock sample was crushed into 40–60 mesh in an agate mortar. Then, the phenocrysts were carefully picked out under a binocular microscope. The separated groundmass was then milled into 200 mesh for the geochemical analyses.

Major element compositions of the whole-rock and groundmass were measured by XRF (X-ray fluorescence spectrometry) on fused glass discs at the Institute of Geology and Geophysics, Chinese Academy of Sciences (IGGCAS), with an analytical uncertainty ranging from 1% to 3% for the elements > 1 wt%, and ~10% for the elements < 1 wt%.

Major element compositions of the clinopyroxene, orthopyroxene and plagioclase phenocrysts were analyzed using the electron microprobe (EMP-1600) at the Guiyang Institute of Geochemistry, Chinese Academy of Sciences (GIGCAS). Analytical conditions include 25 kV accelerating voltage and 10nA beam current focused to a 10 μm spot on the mineral surface. The detection limits for the major elements are 0.01 wt%. Analytical reproducibility was within 2%. The uncertainly of △Mg# for clinopyroxene and orthopyroxene caused by 1 sigma error of the EPMA analysis is less than 2. Quantitative wavelength-dispersive spectrometry (WDS) analysis for the clinopyroxene phenocrysts were conducted using an accelerating voltage of 15 kv, a beam current of 20 nA and a spot size of 1 μm.

5. Results

5.1. Whole-rock and groundmass geochemical compositions

The least altered trachyandesite (lava flow 1) and trachyte (lava flow 2) samples have LOI (loss on ignition) contents of < 0.6 wt% (Table 1). All the major element data were recalculated to a 100 wt% volatile-free basis. In the TAS classification diagram (Fig. 2a), samples from the lava flow 1 and 2 are classified as trachyandesite and trachyte, respectively, consistent with the petrographic classification. All the whole-rock and groundmass compositions of the two rock types plot on/close to the boundary between the high-K calc-alkaline and shoshonitic fields (Fig. 2b). Volcanic rocks from the two lava flows have whole-rock SiO_2 and total alkali contents of 58.3–62.4 wt% and 7.2–7.7 wt%, respectively. The rocks have relatively narrow ranges of MgO (2.7–3.8 wt%), Fe_2O_{3Total} (5.3–6.5 wt%), CaO (4.5–5.8 wt%) and TiO_2 (0.9–1.2 wt%) (Table 1). In the Harker diagrams (Fig. 3), MgO, Fe_2O_{3Total} and CaO show good negative correlations with SiO_2. Moreover, SiO_2 shows strongly positive correlation with the total alkali contents. In general, volcanic rocks of lava flow 1 contain higher MgO and Fe_2O_{3Total} contents than those of lava flow 2. The volcanic groundmass contains lower MgO, Fe_2O_{3Total} and CaO, but higher K_2O and Na_2O contents than the whole-rock compositions (Fig. 3). Similar to the whole-rock compositions, groundmass of lava flow 1 is less evolved than that of lava flow 2.

5.2. Mineral compositions

As above-mentioned, clinopyroxene phenocrysts from the Heikongshan volcanic rocks show (1) reverse, (2) oscillatory, and (3) normal zoning patterns. The compositional variability of clinopyroxene

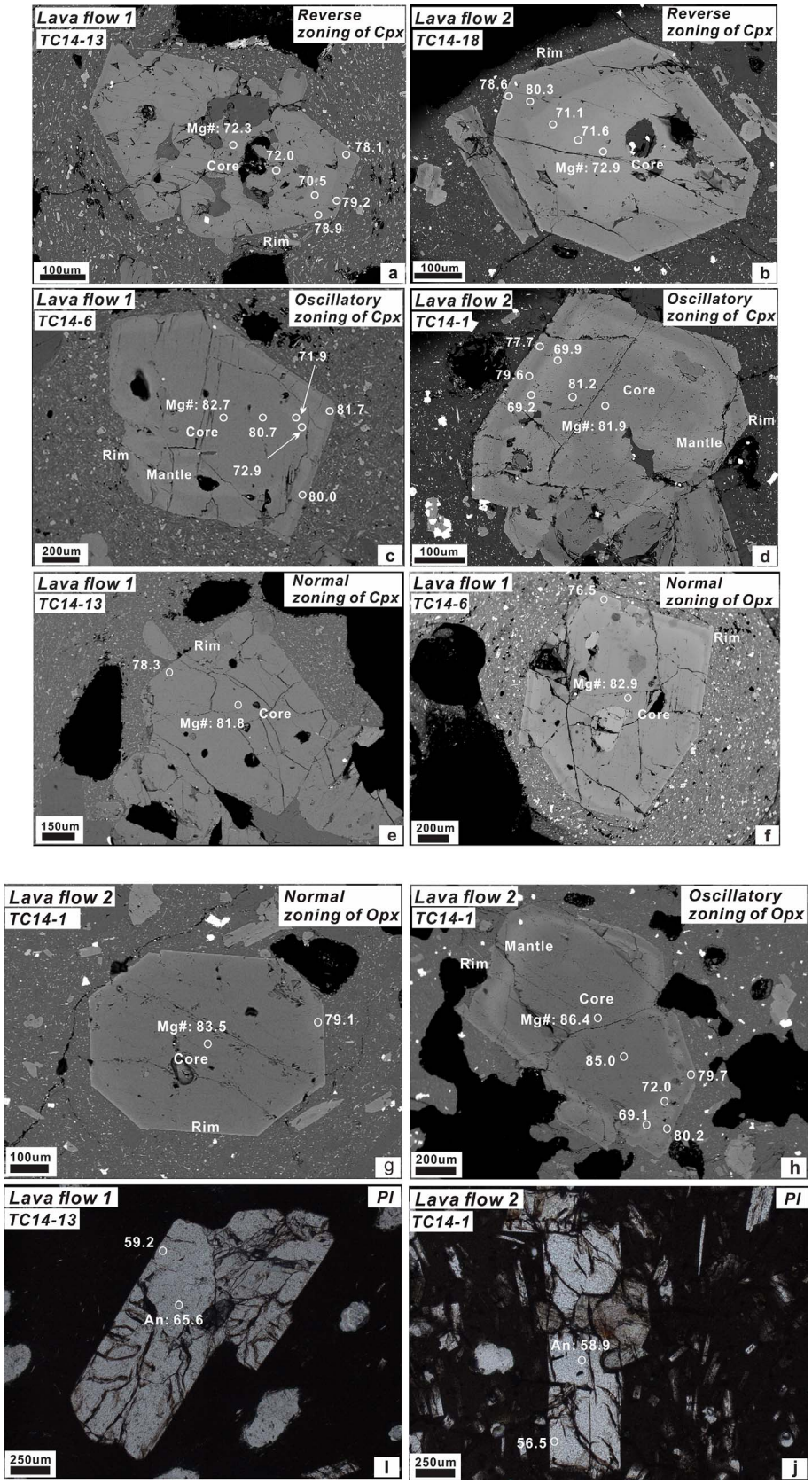

Fig. 4. Representative BSE images and microphotographs (plane-polarized light) of phenocrysts in two lava flows: (a), (c) and (e) the reverse, oscillatory and normal zoning of clinopyroxene phenocrysts in flow 1; (b) and (d) reverse and oscillatory zoning of clinopyroxene phenocrysts in flow 2; (f) normal zoning of orthopyroxene phenocrysts in flow 1; (g) and (h) normal and oscillatory zoning of orthopyroxene phenocrysts in flow 2; (i) and (j) the plagioclase phenocrysts in two lava flows. (white circles in a ~ j denote the EPMA spots; Mg# = Mg/(Mg + Fe^{2+}), An = Ca/(Ca + Na + K), Cpx = clinopyroxene, Opx = orthopyroxene, Pl = plagioclase).

is general expressed as Mg# (i.e., Mg/(Mg + Fe^{2+})*100 = 69–83, in which the Fe^{2+} content is calculated using the equation listed in Lindsley (1983)) (Fig. 7a–f; Appendix II). For lava flow 1, the reversely-zoned clinopyroxene shows abrupt increase in Mg# and Cr, and decrease in Ti from core to rim (Figs. 4a and 7a–b; Appendix II). The Mg# of the core also decreases gradually from inner part to outer part (Fig. 4a). The oscillatory-zoned clinopyroxene has commonly high-Mg#, Cr-rich and Ti-poor core and rim, as well as low-Mg#, Cr-poor

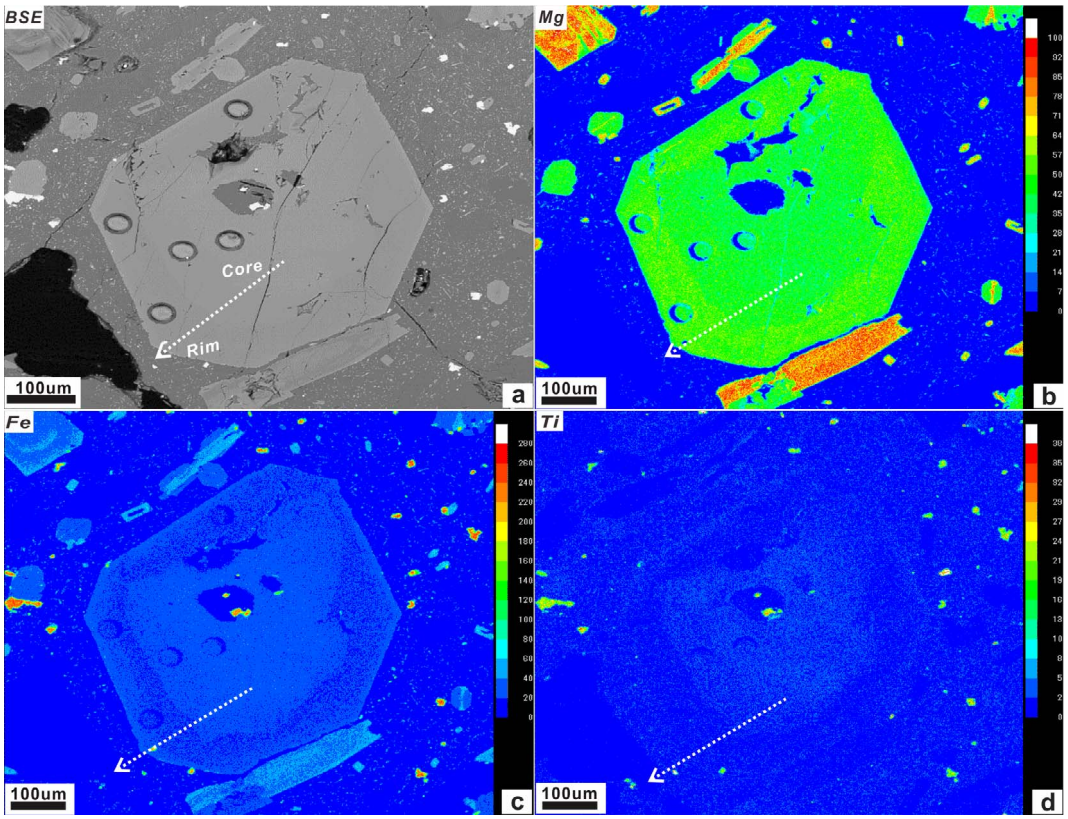

Fig. 5. BSE image and qualitative WDS maps of Mg, Fe, and Ti in an enhedral clinopyroxene phenocryst of sample TC14-18 (lava flow 2). This phenocryst displays reverse zoning. The color contrast of the maps have been adjusted to distinguish the zoning patterns, and thus the colors are not necessarily comparable between maps or with the clinopyroxene elemental maps in other figures. Warm and cool colors represent high and low concentrations, respectively. Small crators in the BSE, Mg and Fe maps are laser spots from previous analyses. White arrow shows the direction from core to rim.

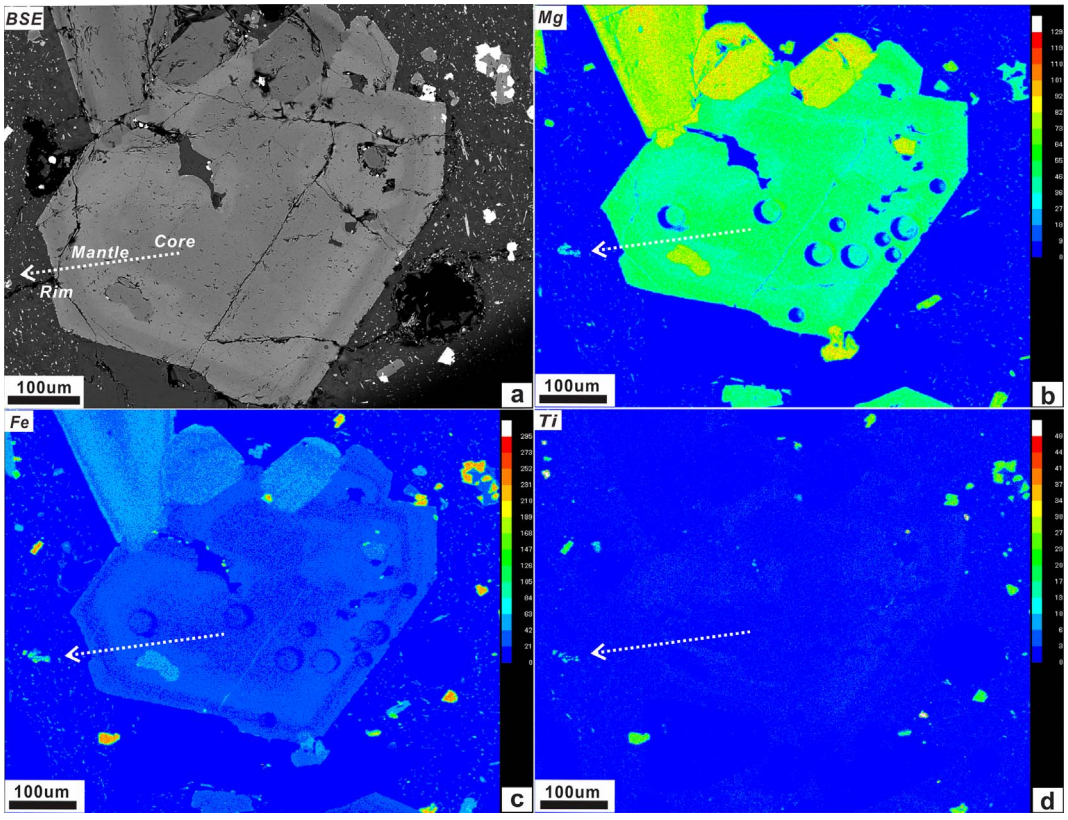

Fig. 6. BSE image and qualitative WDS maps of Mg, Fe and Ti in a clinopyroxene phenocryst of sample TC14-1 (lava flow 2). This phenocryst displays oscillatory zoning with varying thickness and jagged borders. Colors and symbols as in Fig. 5.

Table 1
Whole-rock and groundmass geochemical compositions for the two lava flows of the Heikongshan volcano (wt%).

Lava flow	Lava 1		Lava 2		Lava 1		Lava 2	
Whole rock/groundmass	Whole Rock				groundmass			
Sample	TC14-6	TC14-13	TC14-1	TC14-18	TC14-6	TC14-13	TC14-1	TC14-18
Major elements (wt%)								
SiO_2	58.47	57.88	62.06	61.47	59.16	59.00	63.39	63.35
TiO_2	1.16	1.17	0.94	0.95	1.14	1.19	0.98	0.99
Al_2O_3	16.61	16.53	15.97	15.79	16.60	16.81	15.65	15.62
Cr_2O_3	0.01	0.01	0.01	0.01	0.00	0.00	0.00	0.00
Fe_2O_{3Total}	6.13	6.41	5.25	5.34	6.08	6.21	5.25	5.31
MnO	0.10	0.11	0.09	0.09	0.10	0.10	0.09	0.09
MgO	3.62	3.74	2.72	2.80	2.99	3.02	2.34	2.29
CaO	5.61	5.72	4.47	4.53	5.25	5.31	3.98	3.95
Na_2O	3.62	3.66	3.52	3.61	3.71	3.77	3.65	3.68
K2O	3.51	3.50	4.02	4.03	3.67	3.72	4.32	4.35
BaO	0.11	0.11	0.09	0.10	0.11	0.12	0.10	0.10
P_2O_5	0.43	0.46	0.35	0.36	0.45	0.48	0.37	0.38
SrO	0.06	0.06	0.05	0.05	0.06	0.06	0.05	0.05
LOI	0.27	0.57	0.28	0.27	0.36	0.38	0.12	0.12
Total	99.71	99.93	99.82	99.40	99.68	100.17	100.29	100.28

Note: LOI = Loss on ignition.

and Ti-rich mantle (Figs. 4c and 7c–d; Appendix II). Similar to the reversely-zoned clinopyroxene, the core of oscillatory-zoned clinopyroxene also shows a gradual Mg# decrease from the inner part (Fig. 4c). Normal-zoned clinopyroxene is characterized by decreasing Mg# and Cr contents from core to rim (Figs. 4e and 7f; Appendix II). Clinopyroxene phenocrysts of all the three zoning types show positive Cr vs. Mg# and negative Ti vs. Mg# correlations (Fig. 7a–f).

Orthopyroxene phenocrysts from the trachyandesite (lava flow 1) have only normal zoning, which show decreasing Mg# and Cr contents from core to rim (Fig. 4f and 7g; Appendix II). Meanwhile, plagioclase phenocrysts from the trachyandesite contain an An-rich core and an An-poor rim (Fig. 4i; Appendix II).

Clinopyroxene phenocrysts from the trachyte (lava flow 2) show similar compositional trends of Cr, Ti and Mg# to their trachyandesite (lava flow 1) counterparts, as well demonstrated in the EMPA elemental maps (Figs. 5 and 6). Orthopyroxene phenocrysts from the trachyte also show oscillatory zoning, with high Mg# and Cr contents in the core and rim, and low Mg# and Cr contents in the mantle (Figs. 4 h and 7h; Appendix II). The normal-zoned orthopyroxene from the trachyte shows similar intra-grain compositional trends to that from the trachyandesite (Fig. 7g). Plagioclase phenocrysts from the trachyte have a narrower composition range (An: 61.4–56.5) than those from the trachyandesite (An: 62.4–52.0) (Appendix II).

6. Discussion

6.1. Petrogenetic implications of the clinopyroxene zoning

Compositional and textural zoning of phenocrysts in lavas has received much attention due to its potential to record magmatic physiochemical conditions (Lofgren, 1974; Pearce, 1984, 1987; Tsuchiyama, 1985; Shore and Fowler, 1996; Shearer et al., 2013; Elardo and Shearer, 2014). Fractional crystallization in a closed magmatic plumbing system generates euhedral and normal-zoned phenocrysts (Carracedo, 1999). In contrast, repeated magma replenishment leads to temperature and compositional fluctuations in magma chambers, leading to the formation of normal-, reverse- and oscillatory-zoned phenocrysts (Streck, 2008). Although the interplay of crystal growth and local chemical diffusion within boundary layer could produce fine-scale oscillatory zoning (< 15 μm thick), formation of thick oscillatory zoning is commonly linked to magma compositional fluctuations resulted from magma replenishment and/or large-scale convection in a stratified magma chamber (Pearce and Kolisnik, 1990; Pearce, 1994; Ginibre et al., 2002a, 2002b; Elardo and Shearer, 2014). In this study, most oscillatory zones of the clinopyroxene phenocrysts are over 50 μm thick (Figs. 4c–d and 6), and the jagged contacts between the various zones in the reversely-/oscillatory-zoned clinopyroxene phenocrysts indicate resorption and thus crystal-melt disequilibrium (Figs. 4a–d, 5, and 6). These textural features are also present in the orthopyroxene phenocrysts (Fig. 4h), which altogether suggest substantial temperature and/or compositional fluctuations in the magma chambers, caused probably by magma replenishment (Nakagawa et al., 2002; Humphreys et al., 2006; Stroncik et al., 2009). Sudden pressure drop during magma ascent would increase the crystallization rate, and leads to normal (rather than reverse) zoning (Stroncik et al., 2009). Decreasing Ti content (from core to rim) in the reversely-zoned clinopyroxene due to pressure rise, although theoretically possible (Adam and Green, 1994), is geologically unrealistic during magma ascent and emplacement. Therefore, the presence of various zoning styles of the pyroxene phenocrysts analyzed reflects primarily temperature and compositional (rather than pressure) fluctuations in the magma chambers beneath the Heikongshan volcano.

High-Mg and high-Cr pyroxene commonly crystallized from less evolved (more mafic) magmas (Streck et al., 2002; Streck, 2008), and Ti contents in pyroxene are more affected by magma compositions than by temperature, pressure or water content (Gaetani et al., 1993; Adam and Green, 1994; Skulski et al., 1994; Streck et al., 2002). The Mg#, Cr and Ti contents are well-correlated in the clinopyroxene phenocrysts analyzed, especially for the reversely- and oscillatory-zoned ones. Therefore, Cr and Ti contents and Mg# values are good indicators for the crystallization conditions of the clinopyroxene from the Heikongshan volcanic rocks. Since Cr is strongly partitioned into clinopyroxene and Ti is mildly incompatible, the inner parts of the crystal should have higher Cr and lower Ti contents than the rims in a stable fractionation environment. The positive Cr vs. Mg# and negative Ti vs. Mg# correlations observed are consistent with the partition coefficients of Cr and Ti between clinopyroxene crystals and mafic magmas (Fig. 7a–f) (D_{Cr} = 3–30, D_{Ti} = 0.29–0.89; Bacon and Druitt, 1988; Villemant, 1988; Adam and Green, 1994; Forsythe et al., 1994; Hauri et al., 1994; Skulski et al., 1994; Yang et al., 2017). However, the compositional variations in the reversely- and oscillatory-zoned clinopyroxene phenocrysts cannot be explained by closed-system fractional crystallization (Figs. 5, 6, and 7a–d).

Composition relationships between the rim and mantle of the oscillatory-zoned clinopyroxene are comparable to those between the rim and core of the reversely-zoned clinopyroxene (Fig. 7a–d; Appendix II). The higher Mg# and Cr contents of the rims (Mg# = 78.1–79.2, Cr_2O_3 = 0.07–0.13 wt%) than those of the cores (Mg# = 70.5–72.3,

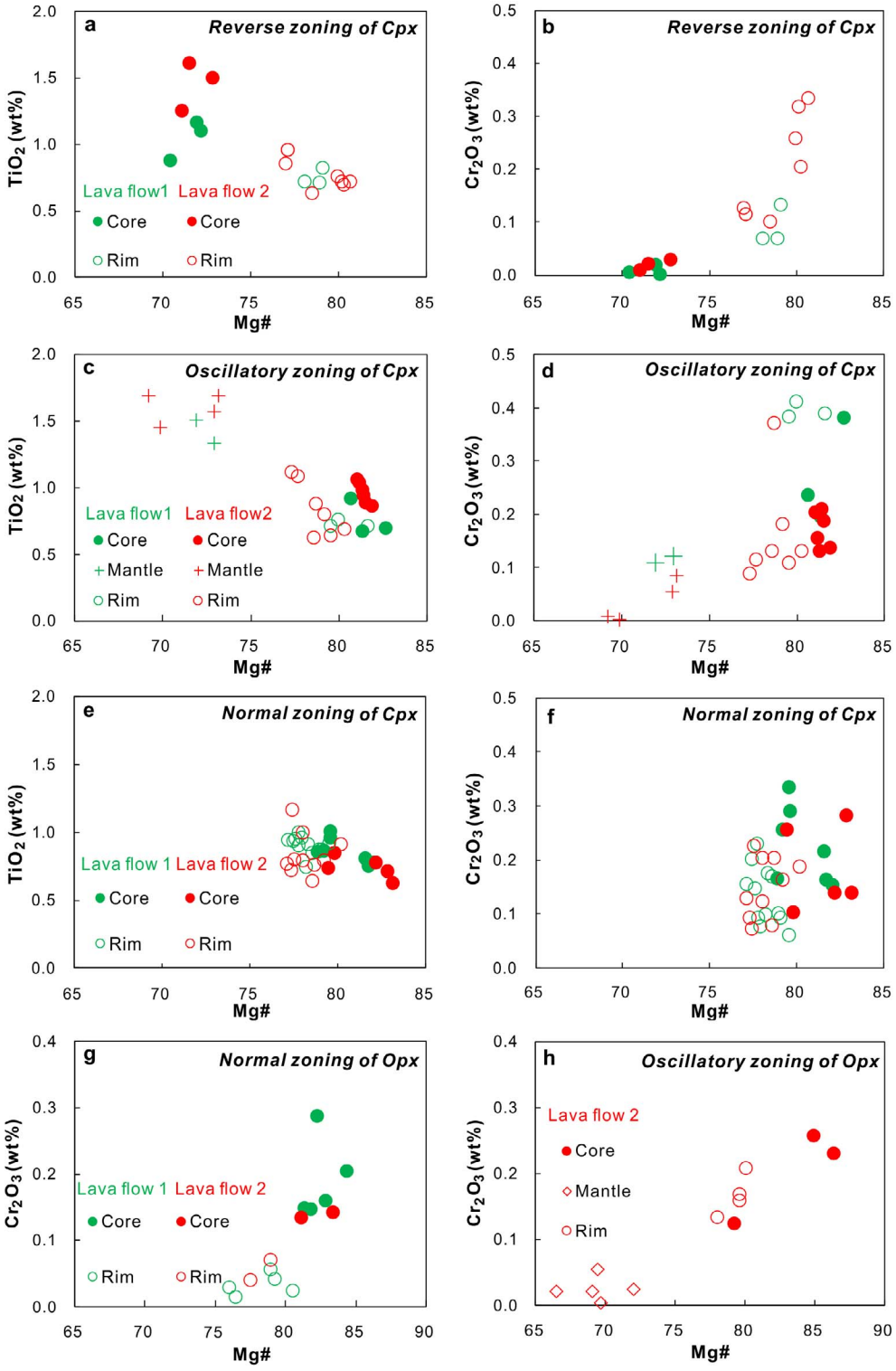

Fig. 7. Compositions of the pyroxene phenocrysts in two lava flows of the Heikongshan volcano. (a), (c) and (e) TiO_2 vs. Mg# of zoned clinopyroxene phenocrysts; (b), (d) and (f) Cr_2O_3 vs. Mg# of zoned clinopyroxene phenocrysts; (g) and (h) Cr_2O_3 vs. Mg# of zoned orthopyroxene phenocrysts. (Mg# = Mg/(Mg + Fe^{+2}), Fe^{+2} is calculated using the equation of Landsley (1983), Cpx = clinopyroxene, Opx = orthopyroxene).

Cr_2O_3 = 0–0.03 wt%) of the reversely-zoned clinopyroxene from the trachyandesite (lava flow 1) (Figs. 4a and 7b; Appendix II) indicate that the replenished magma was relatively less evolved. This suggests that the core of the reversely-zoned clinopyroxene and the mantle of the oscillatory-zoned clinopyroxene were likely formed from a more evolved magma. Although the cores of the oscillatory-zoned clinopyroxene contain higher Mg# and Cr contents (Mg# = 80.7–82.7, Cr_2O_3 = 0.23–0.38 wt%) than the mantles (Mg# = 71.9–72.9, Cr_2O_3 = 0.11–0.12 wt%) (Figs. 4c and 7d; Appendix II), the jagged contact between them suggests that the latter was grown on the resorptive boundary of the former during magma replenishment (Figs. 4c and 7d). The magma that equilibrated with the oscillatory-zoned clinopyroxene mantle had Mg# values of 40.9–42.1, as calculated with the clinopyroxene Mg# values and the Fe-Mg exchange coefficients from Putirka et al. (2003). Such magma compositions were more evolved and in disequilibrium with the clinopyroxene cores. Thus, we infer that there were multiphase magma replenishment into the magma chamber before the eruption of the lava flow 1. The same is true for lava flow 2 due to the similar textural and compositional variations of the reversely-, oscillatory- and normal-zoned clinopyroxene

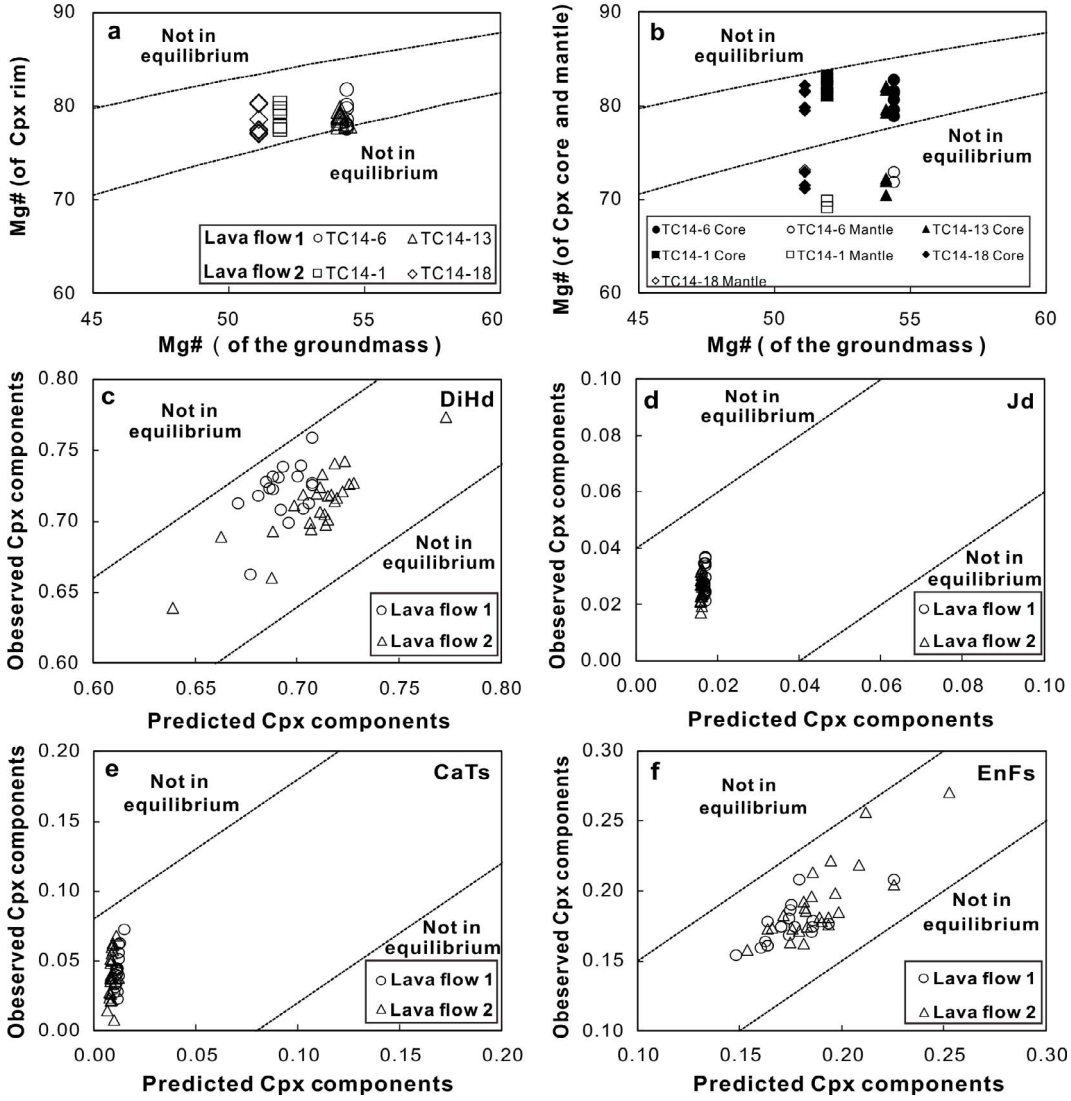

Fig. 8. Clinopyroxene-melt equilibrium tests: (a) and (b) Mg# of clinopyroxene cores and rims for all investigated samples vs. Mg# of groundmass. Each symbol represents a single EMP analysis. Black curves represent the range of equilibrium compositions between clinopyroxene and groundmass using a distribution coefficient of 0.275 ± 0.067 from Putirka et al. (2003). (c)–(f) Measured and calculated values for clinopyroxene phenocrysts components (mole fraction). (Cpx = clinopyroxene, DiHd = diopside + hedenbergite, EnFs = enstatite + ferrosilite, CaTs = Ca-Tschermak, and Jd = jadeite. The equilibrium envelopes are marked by the SEE values, which are for DiHd ± 0.06 SEE; EnFs ± 0.05 SEE from Mollo et al. (2013); CaTs ± 0.08 2SEE and Jd ± 0.04 2SEE from Putirka (1999)).

phenocrysts of the trachyte (Figs. 4–7). Moreover, the compositional variations of the plagioclase phenocrysts from dacite in this region were also resulted from magma recharge and mixing (Gao et al., 2015). To conclude, we propose that magma replenishment and mixing have played an important role in the compositional evolution and phenocryst growth in the magma chambers beneath the Heikongshan volcano, and probably also other Cenozoic volcanoes in the Tengchong area.

6.2. Clinopyroxene-melt thermobarometry

To better understand the magma chamber processes beneath the Heikongshan volcano, clinopyroxene-melt thermobarometry was used to constrain the T-P (temperature-pressure) conditions of the clinopyroxene phenocryst crystallization. Clinopyroxene-melt thermobarometer is more accurate in T-P calculations for the phenocryst crystallization (than plagioclase- or orthopyroxene-liquid thermobarometer) due to the wider applicability and lower SEE (standard error of estimate) values of the former (Putirka and Condit, 2003; Caprarelli and Reidel, 2005; Putirka, 2005, 2008; Barker et al., 2009; Hammer et al., 2016). The clinopyroxene-melt thermobarometer of Putirka et al. (2003) is employed in this study, which is based on the jadeite-diopside/hedenbergite exchange under equilibrium between clinopyroxene crystals and mafic to felsic melts (SiO_2 = 51–71.3 wt%). This thermobarometer has an estimated standard error of 1.7 kbar and 33 °C and no systematic bias (Putirka et al., 2003).

Geochemical compositions of the groundmass (or whole-rock with very few phenocrysts) can generally be regarded as the compositions of the melt equilibrated with the phenocrysts (Dahren et al., 2012; Keiding and Sigmarsson, 2012; Keiding et al., 2013). Since the Heikongshan volcanic rocks contain > 5% phenocrysts, the groundmass was carefully separated from the phenocrysts. Our data show that the groundmass contains slightly higher SiO_2 and K_2O, and lower MgO and CaO than the whole-rock compositions (Figs. 2 and 3). The clinopyroxene phenocryst rims formed in the final magmatic stage before the volcanic eruptions can be regarded as in equilibrium with the groundmass. Fe–Mg exchange equilibrium between the clinopyroxene phenocryst rims and groundmasses was tested using the equation of $K_D^{Cpx\text{-}liq}$ ($K_D = (X_{FeO}/X_{MgO})_{Cpx}/(X_{FeO}/X_{MgO})_{liq}$) (Damasceno et al., 2002; Villiger et al., 2007; Longpré et al., 2008). As shown in Fig. 8a and b, the K_D values between the clinopyroxene phenocryst rims and the groundmass

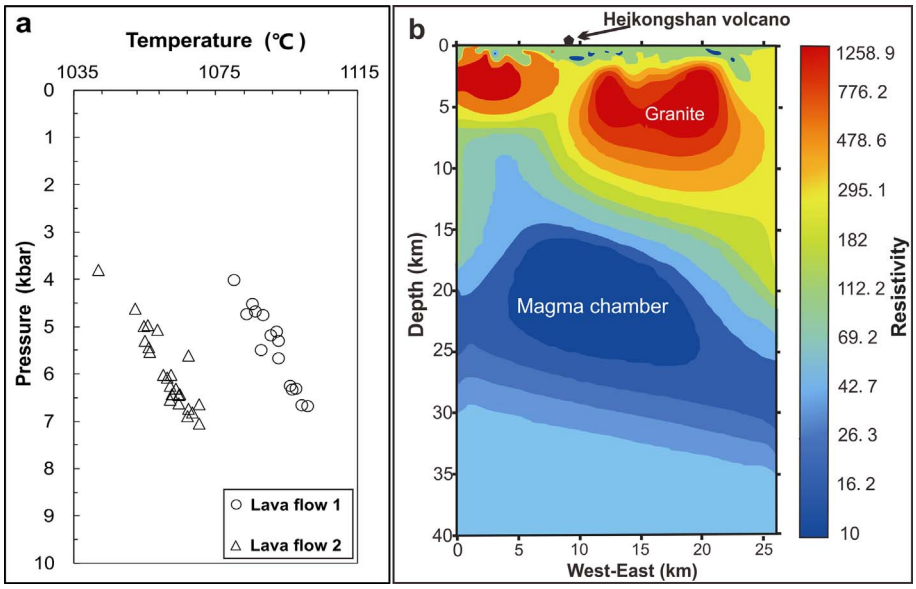

Fig. 9. (a) Pressure and temperature of clinopyroxene crystallization calculated by chemical thermobarometry (Putirka et al., 2003). Each sign denotes data point from clinopyroxene-melt pair. (b) A magnetotelluric profile across Heikongshan volcano (modified from Jiang et al., 2012). The blue region (depths of 12–30 km) in Fig. 9b represents the low resistivity zone, which probably indicate unconsolidated magma chambers. (For interpretation of the references to colour in this figure legend, the reader is referred to the web version of this article.)

range from 0.250 to 0.352, most of which plot in the equilibrium belt (K_D = 0.275 ± 0.067, Putirka et al., 2003). Fig. 8c–f illustrates that the "observed mineral components" of the clinopyroxene phenocryst rims are well consistent with the "predicted mineral components" using the groundmass compositions and estimated T-P conditions of this study, according to the model proposed by Putirka (1999) and Mollo et al. (2013). This indicates that the clinopyroxene-melt pairs may have been close to total equilibrium for calculating the T-P conditions of the magma chamber(s) beneath the Heikongshan volcano.

According to the T-P calculations above-mentioned, crystallization of the clinopyroxene phenocryst rims of both lava flow 1 and 2 occurred under similar pressures (3.8–7.1 kbar, mostly 4.5–7.0 kbar; Fig. 9a; Appendix III). This means that the magma chamber(s) of the Heikongshan volcano was emplaced at depths of around 14–21 km before the eruptions of lava flows 1 and 2. This is well consistent with the large low-resistivity body at around 12–30 km beneath the Heikongshan volcano identified by magnetotelluric survey (Fig. 9b; Jiang et al., 2012), which further implies that the magma chamber(s) beneath the volcano is yet to be totally consolidated. Our thermobarometric calculations indicate that the crystallization temperatures of the clinopyroxene phenocryst rims from the lava flow 1 (1080–1101 °C) are higher than those from the lava flow 2 (1041–1070 °C) (Fig. 9a; Appendix III). This is consistent with the fact that the groundmass of the lava flow 1 contains higher MgO, Fe_2O_{3Total} and CaO contents, and lower SiO_2 and (Na_2O + K_2O) contents than those of lava flow 2 (Figs. 2 and 3). This again demonstrates that the magma chamber beneath the Heikongshan volcano had experienced multiphase replenishment of magmas with different temperatures and compositions.

6.3. Mechanism for the Heikongshan volcanic eruption and future volcanic hazard assessment

Magma storage and replenishment of the magma chambers beneath volcanoes are key elements to understand the volcanic behaviors and to predict potential future volcanic eruptions (Morgan et al., 2004). A closed-system magma chamber could rarely cause volcanic eruptions because the pressure, temperature and magma volume decrease with time (Stasiuk et al., 1993), and the opposite is true for an open magmatic plumbing system (Sparks et al., 1977; Eichelberger, 1995; Murphy et al., 1998, 2000; Tepley et al., 2000; Samaniego et al., 2011), such as the Heikongshan magmatic plumbing system in this study.

Previous K–Ar dating had identified a series of volcanic eruptions at Heikongshan from the late Pleistocene (ca. 482 ka) to the Holocene (ca. 7 ka) (Mu et al. 1987; Nakai et al. 1993; Li et al. 2000). Jiang et al. (2012) has proposed that the low-resistivity body beneath the Heikongshan volcano likely represents an active magma chamber. Thus, although the Tengchong volcanoes have been dormant for hundreds of years (latest eruption reported at Dayingshan volcano (south of Heikongshan) in 1609 CE), they still have potential to erupt again in the future. Additionally, the Tengchong area shows high geothermal gradient with high $^3He/^4He$ ratios (Fig. 1b), which suggest the increasing presence of mantle-derived helium in recent years (Zhao et al., 2012). The strike-slip faulting that control the Cenozoic volcano distributions in the Tengchong area are still active, and have generated the medium-strong earthquakes in this region, such as the Yinjiang earthquake (M 5.8) in 2011 (Lei et al., 2012a, 2012b; Zhou et al., 2012). Therefore, the possibility of future volcano eruptions in the Tengchong area should not be dismissed, especially because of the large resident/tourist population in the area.

7. Conclusions

(1) The presence of reversely- and oscillatory-zoned clinopyroxene phenocrysts indicates that the magma chamber(s) beneath the Heikongshan volcano had experienced multiphase magma mixing and replenishment, which eventually triggered the volcanic eruptions during the late Pleistocene to Holocene.
(2) Thermobarometric calculations on the rims of the clinopyroxene phenocrysts indicate that the magma chamber(s) beneath the Heikongshan volcano may have emplaced at depths of 14 to 21 km prior to the eruptions of lava flows 1 and 2.
(3) Although there were no volcanic eruptions in the Tengchong area since 1609 CE, the possibility of future volcano eruptions still exists if the magma chamber(s) (likely to be active) is disturbed by the regional strike-slip faulting.

Acknowledgements

This work was funded by the National Key Research and Development Program of China (2016YFC0600503) and the Strategic Priority Research Program (B) of the Chinese Academy of Sciences (XDB18000000). Professor Mei-Fu Zhou (Editor-in-Chief) and two anonymous reviewers are thanked for their insightful comments and suggestions.

Appendix A. Supplementary material

Supplementary data associated with this article can be found, in the online version, at https://doi.org/10.1016/j.jseaes.2017.12.029.

References

Adam, J., Green, T.H., 1994. The effects of pressure and temperature on the partitioning of Ti, Sr and REE between amphibole, clinopyroxene and basanitic melts. Chem. Geol. 117, 219–233.

Anderson, A.T., 1984. Probable relations between plagioclase zoning and magma dynamics, Fuego Volcano,. GuatemalaAm. Mineral. 69, 660–676.

Bacon, C.R., Druitt, T.H., 1988. Compositional evolution of the zoned calcalkaline magma chamber of Mount Mazama, Crater Lake, Oregon. Contrib. Mineral. Petrol. 98, 224–256.

Barker, A.K., Holm, P.M., Peate, D.W., Baker, J.A., 2009. Geochemical stratigraphy of submarine lavas (3–5 Ma) from the Flamengos Valley, Santiago, Southern Cape Verde Islands. J. Petrol. 50, 169–193.

Caprarelli, G., Reidel, S.P., 2005. A clinopyroxene–basalt geothermobarometry perspective of Columbia Plateau (NW-USA) Miocene magmatism. Terra. Nova. 17, 265–277.

Carracedo, J.C., 1999. Growth, structure, instability and collapse of Canarian volcanoes and comparisons with Hawaiian volcanoes. J. Volcanol. Geotherm. Res. 94, 1–19.

Chung, S.L., Chu, M.F., Zhang, Y.Q., Xie, Y.W., Lo, C.H., Lee, T., Lan, C.Y., Li, X.H., Zhang, Q., Wang, Y.Z., 2005. Tibetan tectonic evolution inferred from spatial and temporal variations in post-collisional magmatism. Earth. Sci. Rev. 68, 173–196.

Dahren, B., Troll, V.R., Andersson, U.B., Chadwick, J.P., Gardner, M.F., Jaxybulatov, K., Koulakov, I., 2012. Magma plumbing beneath Anak Krakatau volcano, Indonesia: evidence for multiple magma storage regions. Contrib. Mineral. Petrol. 163, 631–651.

Damasceno, D., Scoates, J.S., Weis, D., Frey, F.A., Giret, A., 2002. Mineral chemistry of mildly alkalic basalts from the 25 Ma Mont crozier section, Kerguelen archipelago: constraints on phenocryst crystallization environments. J. Petrol. 43, 1389–1413.

Eichelberger, J.C., 1995. Silicic volcanism: ascent of viscous magmas from crustal reservoirs. Annu. Rev. Earth. Planet. Sci. 23, 41–64.

Elardo, S.M., Shearer, C.K., 2014. Magma chamber dynamics recorded by oscillatory zoning in pyroxene and olivine phenocrysts in basaltic lunar meteorite Northwest Africa 032. Am. Mineral. 99, 355–368.

Forsythe, L.M., Nielsen, R.L., Fisk, M.R., 1994. High-field-strength element partitioning between pyroxene and basaltic to dacitic magmas. Chem. Geol. 117, 107–125.

Gaetani, G.A., Grove, T.L., Bryan, W.B., 1993. The influence of water on the petrogenesis of subduction-related igneous rocks. Nature 365, 332–334.

Gao, J.F., Zhou, M.F., Robinson, P.T., Wang, C.Y., Zhao, J.H., Malpas, J., 2015. Magma mixing recorded by Sr isotopes of plagioclase from dacites of the Quaternary Tengchong volcanic field, SE Tibetan. J. Asian Earth Sci. 98, 1–17.

Gerbe, M.C., Thouret, J.C., 2004. Role of magma mixing in the petrogenesis of tephra erupted during the 1990–98 explosive activity of Nevado Sabancaya, southern Peru. Bull. Volcanol. 66, 541–561.

Ginibre, C., Kronz, A., Wörner, G., 2002a. High-resolution quantitative imaging of plagioclase composition using accumulated backscattered electron images: new constraints on oscillatory zoning. Contrib. Mineral. Petrol. 142, 436–448.

Ginibre, C., Wörner, G., Kronz, A., 2002b. Minor- and trace-element zoning in plagioclase: implications for magma chamber processes at Parinacota volcano, northern Chile. Contrib. Mineral. Petrol. 143, 300–315.

Ginibre, C., Worner, G., Kronz, A., 2007. Crystal zoning as an archive for magma evolution. Elements 3, 261–266.

Guo, Z.F., Cheng, Z.H., Zhang, M.L., Zhang, L.H., Li, X.H., Liu, J.Q., 2015. Post-collisional high-K calc-alkaline volcanism in Tengchong volcanic field, SE Tibet: constraints on Indian eastward subduction and slab detachment. J. Geol. Soc. 172, 624–640.

Hammer, J., Jacob, S., Welsch, B., Hellebrand, E., Sinton, J., 2016. Clinopyroxene in postshield Haleakala ankaramite: 1. Efficacy of thermobarometry. Contrib. Mineral. Petrol. 171, 1–23.

Hauri, E.H., Wagner, T.P., Grove, T.L., 1994. Experimental and natural partitioning of Th, U, Pb and other trace elements between garnet, clinopyroxene and basaltic melts. Chem. Geol. 117, 149–166.

He, R., Zhao, D., Gao, R., Zheng, H., 2010. Tracing the Indian lithospheric mantle beneath central Tibetan Plateau using teleseismic tomography. Tectonophysics 491 (1–4), 230–243.

Hibbard, M.J., 1981. The magma mixing origin of mantled feldspars. Contrib. Mineral. Petrol. 76, 158–170.

Huangfu, G., Jiang, C.S., 2000. Study on tengchong volcanic activity (in Chinese with English abstract). Yunan Technol Press, Kunming, pp. 18–76.

Humphreys, M.C.S., Blundy, J.D., Sparks, R.S.J., 2006. Magma evolution and open-system processes at Shiveluch volcano: insights from phenocryst zoning. J. Petrol. 47, 2303–2334.

Huang, X.W., Zhou, M.F., Wang, C.Y., Robinson, P.T., Zhao, J.H., Qi, L., 2013. Chalcophile element constraints on magma differentiation of Quaternary volcanoes in Tengchong, SW, China. J. Asian Earth Sci. 76, 1–11.

Jiang, M., Tan, H.D., Zhang, Y.W., Peng, M., Li, Q.Q., Zhang, L.S., Xu, L.H., Wang, W., 2012. Geophysical mode of Mazhan-Gudong magma chamber in Tengchong volcano-tectonic Area (in Chinese with English abstract). Acta Petrologica Sinica 33, 731–739.

Kahl, M., Chakraborty, S., Costa, F., Pompilio, M., 2011. Dynamic plumbing system beneath volcanoes revealed by kinetic modeling, and the connection to monitoring data: An example from Mt. Etna. Etna. Earth Planet Sci. Lett. 308, 11–22.

Keiding, J.K., Frei, O., Renno, A.D., Veksler, I.V., Trumbull, R.B., 2013. Conditions of magma crystallization in the Henties Bay-Outjo dyke swarm, Namibia: Implications for the feeder system of continental flood basalts. Lithos 179, 16–27.

Keiding, J.K., Sigmarsson, O., 2012. Geothermobarometry of the 2010 Eyjafjallajökull eruption: New constraints on Icelandic magma plumbing systems. J. Geophys. Res. 117, B00C09.

Kornfeld, D., Sonntag, B.L., Gast, S., Matthes, J., Ratschbacher, L., Pfänder, J.A., Eckert, S., Liu, D.L., Appel, E., Ding, L., 2014. Apparent paleomagnetic rotations reveal Pliocene-Holocene internal deformation of the Tengchong Block, southeastern Tibetan Plateau. J. Asian. Earth. Sci. 96, 1–16.

Le Maitre, R.W., Bateman, P., Dudek, A., Keller, J., Lameyre, J., Le Bas, M.J., Sabine, P.A., Schmid, R., Sorensen, H., Streckeisen, A., Woolley, A.R., Zanettin, B., 1989. A classification of igneous rocks and glossary of terms. Blackwell, Oxford.

Lei, J.S., Xie, F.R., Mishra, O.P., Lu, Y.Z., Zhang, G.W., Li, Y., 2012a. The 2011 Yingjiang, China, earthquake: a volcano-related fluid-driven earthquake? Bull. Seismol. Soc. Am. 102, 417–425.

Lei, J.S., Zhang, G.W., Xie, F.R., Li, Y., Su, Y.J., Liu, L.F., Ma, H.H., Zhang, J.W., 2012b. Relocation of the 10 March 2011 Yingjiang, China, earthquake sequence and its tectonic implications. Earthq. Sci. 25, 103–110.

Lei, J.S., Zhao, D.P., Su, Y.J., 2009. Insight into the origin of the Tengchong intraplate volcano and seismotectonics in southwest China from local and teleseismic data. J. Geophys. Res. 114, B05302.

Li, C., van Der Hilst, R.D., Meltzer, A.S., Engdahl, E.R., 2008. Subduction of the Indian lithosphere beneath the Tibetan Plateau and Burma. Earth. Planet. Sci. Lett. 274, 157–168.

Li, D.M., Li, Q., Chen, W.J., 2000. Volcanic activity of Tengchong since Pliocene (in Chinese with English abstract). Acta Petrologica Sinica 16, 362–370.

Li, X., Liu, J.Q., 2012. A study on the geochemical characteristics and petrogenesis of Holocene volcanic rocks in the Tengchong volcanic eruption field, Yunnan Province, SW China (in chinese with English abstract). Acta Petrologica Sinica 28, 1507–1516.

Lindsley, D.H., 1983. Pyroxene thermometry. Am. Mineral. 68, 477–493.

Liu, J.Q., 1999. Volcanoes of china. Science Press, Beijing.

Lofgren, G., 1974. An experimental study of plagioclase crystal morphology; isothermal crystallization. Am. J. Sci. 274, 243–273.

Longpré, M.A., Troll, V.R., Hansteen, T.H., 2008. Upper mantle magma storage and transport under a Canarian shield-volcano, Teno, Tenerife (Spain). J. Geophys. Res. 113, B08203.

Longpré, M.A., Klugel, A., Diehl, A., Stix, J., 2014. Mixing in mantle magma reservoirs prior to and during the 2011–2012 eruption at El Hierro, Canary Islands. Geology 42, 315–318.

Mo, X.X., Zhao, Z.D., Deng, J.F., Flower, M., Yu, X.H., Luo, Z.H., Li, Y.G., Zhou, S., Dong, G.C., Zhu, D.C., Wang, L.L., 2006. Petrology and geochemistry of postcollisional volcanic rocks from the Tibetan plateau: Implications for lithosphere heterogeneity and collision-induced asthenospheric mantle flow. In: Dilek,Y., Pavlides, S., (Eds.), Postcollisional tectonics and magmatism in the Mediterranean Region and Asia, vol 409. Geological Society of America Special Paper, pp. 507–530.

Mollo, S., Putirka, K., Misiti, V., Soligo, M., Scarlato, P., 2013. A new test for equilibrium based on clinopyroxene–melt pairs: Clues on the solidification temperatures of Etnean alkaline melts at post-eruptive conditions. Chem. Geol. 352, 92–100.

Morgan, D.J., Blake, S., 2006. Magmatic residence times of zoned phenocrysts: introduction and application of the binary element diffusion modelling (BEDM) technique. Contrib. Mineral. Petrol. 151, 58–70.

Morgan, D.J., Blake, S., Rogers, N.W., 2004. Time scales of crystal residence and magma chamber volume from modelling of diffusion profiles in phenocrysts: Vesuvius 1944. Earth Planet. Sci. Lett. 222, 933–946.

Mu, Z.G., Tong, W., Curtis, G.H., 1987. Times of volcanic activity and origin of magma in Tengchong geothermal area, west Yunnan province (in Chinese with English abstract). Acta Geophysics Sinica 30, 261–270.

Murphy, M.D., Sparks, R.S.J., Barclay, J., Carroll, M.R., Brewer, T.S., 2000. Remobilization of Andesite Magma by Intrusion of Mafic Magma at the Soufriere Hills Volcano, Montserrat, West Indies. J. Petrol. 41, 21–42.

Murphy, M.D., Sparks, R.S.J., Barclay, J., Carroll, M.R., Lejeune, A.M., Brewer, T.S., Macdonald, R., Black, S., Young, S., 1998. The role of magma mixing in triggering the current eruption at the Soufriere Hills Volcano, Montserrat, West Indies. Geophys. Res. Lett. 25, 3433–3436.

Nakagawa, M., Hiraga, N., Furukawa, R., 2011. Formation of a zoned magma chamber and its temporal evolution during the historic eruptive activity of Tarumai Volcano, Japan: Petrological implications for a long-term forecast of eruptive activity of an active volcano. J. Volcanol. Geotherm. Res. 205, 1–16.

Nakagawa, M., Wada, K., Wood, C.P., 2002. Mixed magmas, mush chambers and eruption triggers: evidence from zoned clinopyroxene phenocrysts in andesitic scoria from the 1995 eruptions of Ruapehu Volcano, New Zealand. J. Petrol. 43, 2279–2303.

Nakai, S.I., Xu, S., Wakita, H., Fujii, N., Nagao, K., Orihashi, Y., Wang, X., Chen, J., Liao, Z., 1993. K-Ar ages of young volcanic rocks from Tengchong area, Western Yunnan, China. Bull. Volcanol. Soc. Jpn. 39, 167–171.

Pearce, T.H., 1984. The analysis of zoning in magmatic crystals with emphasis on olivine. Contrib. Mineral. Petrol. 86, 149–154.

Pearce, T.H., 1987. The theory of zoning patterns in magmatic minerals using olivine as an example. Contrib. Mineral. Petrol. 97, 451–459.

Pearce, T.H., 1994. Recent work on oscillatory zoning in plagioclase. In: Parsons, I. (Ed.), Feldspars and Their Reactions (NATO Advanced Study Inst). Kluwer, Dordrecht, pp. 313–346.

Pearce, T.H., Kolisnik, A.M., 1990. Observations of plagioclase zoning using interference imaging. Earth. Sci. Rev. 29, 9–26.

Putirka, K., 1999. Clinopyroxene + liquid equilibria to 100 kbar and 2450 K. Contrib. Mineral. Petrol. 135, 151–163.

Putirka, K., Condit, C.D., 2003. Cross section of a magma conduit system at the margin of

the Colorado Plateau. Geology 31, 701–704.
Putirka, K., 2005. Igneous thermometers and barometers based on plagioclase + liquid equilibria: Tests of some existing models and new calibrations. Am. Mineral. 90, 336–346.
Putirka, K., 2008. Thermometers and barometers for volcanic systems. Rev. Mineral. Geochem. 69, 61–120.
Putirka, K., Mikaelian, H., Ryerson, F., Shaw, H., 2003. New clinopyroxene-liquid thermobarometers for mafic, evolved, and volatile-bearing lava compositions, with applications to lavas from Tibet and the Snake River Plain, Idaho. Am. Mineral. 88, 1542–1554.
Rivera, M., Thouret, J.C., Samaniego, P., Pennec, J.L.L., 2014. The 2006–2009 activity of the Ubinas volcano (Peru): Petrology of the 2006 eruptive products and insights into genesis of andesite magmas, magma recharge and plumbing system. J. Volcanol. Geotherm. Res. 270, 122–141.
Samaniego, P., Pennec, J.L.L., Robin, C., Hidalgo, S., 2011. Petrological analysis of the pre-eruptive magmatic process prior to the 2006 explosive eruptions at Tungurahua volcano (Ecuador). J. Volcanol. Geotherm. Res. 199, 69–84.
Shearer, C.K., Aaron, P.M., Burger, P.V., Guan, Y., Bell, A.S., Papike, J.J., 2013. Petrogenetic linkages among fO2, isotopic enrichments-depletions and crystallization history in Martian basalts. Evidence from the distribution of phosphorus in olivine megacrysts. Geochim. Cosmochim. Acta 120, 17–38.
Shore, M., Fowler, A.D., 1996. Oscillatory zoning in minerals: A common phenomenon. Can. Mineral. 34, 1111–1126.
Skulski, T., Minarik, W., Watson, E.B., 1994. High-pressure experimental trace-element partitioning between clinopyroxene and basaltic melts. Chem. Geol. 117, 127–147.
Sparks, S.R.J., Sigurdsson, H., Wilson, L., 1977. Magma mixing: a mechanism for triggering acid explosive eruptions. Nature 267, 315–318.
Stasiuk, M.V., Jaupart, C., Sparks, R.S.J., 1993. On the variations of flow rate in non-explosive lava eruptions. Earth. Planet. Sci. Lett. 114, 505–516.
Streck, M.J., 2008. Mineral textures and zoning as evidence for open system processes. Rev. Mineral. Geochem. 69, 595–622.
Streck, M.J., Dungan, M.A., Malavassi, E., Reagan, M.K., Bussy, F., 2002. The role of basalt replenishment in the generation of basaltic andesites of the ongoing activity at Arenal volcano, Costa Rica: evidence from clinopyroxene and spinel. Bull. Volcanol. 64, 316–327.
Stroncik, N.A., Klügel, A., Hansteen, T.H., 2009. The magmatic plumbing system beneath El Hierro (Canary Islands): constraints from phenocrysts and naturally quenched basaltic glasses in submarine rocks. Contrib. Mineral. Petrol. 157, 593–607.
Sun, Y.J., Wu, Z.H., Ye, P.S., Zhang, H., Li, H.L., Tong, Y.B., 2016. Dynamics of the Tengchong volcanic region in the southeastern Tibetan plateau: A numerical study. Tectonophysics 683, 272–285.
Tepley, F.J., Davidson, J.P., Tilling, R.I., Arth, J.G., 2000. Magma mixing, recharge and eruption histories recorded in plagioclase phenocrysts from El Chichón Volcano, Mexico. J. Petrol. 41, 1397–1411.
Tsuchiyama, A., 1985. Dissolution kinetics of plagioclase in the melt of the system diopside-albite-anorthite, and origin of dusty plagioclase in andesites. Contrib. Mineral. Petrol. 89, 1–16.
Tucker, R.T., Zou, H.B., Fan, Q.C., Schmitt, A.K., 2013. Ion microprobe dating of zircons from active Dayingshan volcano, Tengchong, SE Tibetan Plateau: Time scales and nature of magma chamber storage. Lithos 172–173, 214–221.
Villemant, B., 1988. Trace element evolution in the Phlegrean Fields (Central Italy): fractional crystallization and selective enrichment. Contrib. Mineral. Petrol. 98, 169–183.
Villiger, S., Ulmer, P., Müntener, O., 2007. Equilibrium and fractional crystallization experiments at 0.7 GPa; the effect of pressure on phase relations and liquid compositions of tholeiitic magmas. J. Petrol. 48, 159–184.
Wang, C.Y., Huangfu, G., 2004. Crustal structure in Tengchong Volcano-Geothermal Area, western Yunnan, China. Tectonophysics 380, 69–87.
Wang, F., Chen, W.J., Peng, Z.C., Zhang, Z.L., Hu, Y.T., 1999. Chronology of young volcanic rocks of Changbaishan Tianchi and Tengchong, China, by using the Uranium-series TIMS method. Geol. Rev. 45, 914–924.
Wang, F., Peng, Z.C., Zhu, R.X., He, H.Y., Yang, L.K., 2006. Petrogenesis and magma residence time of lavas from Tengchong volcanic field (China): Evidence from U series disequilibria and $^{40}Ar/^{39}Ar$ dating. Geochem. Geophys. Geosyst. 7, Q01002.
Wang, Y., Zhang, X.M., Jiang, C.S., Wei, H.Q., Wan, J.L., 2007. Tectonic controls on the late Miocene-Holocene volcanic eruptions of the Tengchong volcanic field along the southeastern margin of the Tibetan plateau. J. Asian. Earth. Sci. 30, 375–389.
Wu, T.F., Zhang, S.X., Li, M.K., Qin, W.B., Zhang, C.Y., 2016. Two crustal flowing channels and volcanic magma migration underneath the SE margin of the Tibetan Plateau as revealed by surface wave tomography. J. Asian. Earth. Sci. 132, 25–39.
Xu, Y., Yang, X.T., Li, Z.W., Liu, J.H., 2012. Seismic structure of the Tengchong volcanic area southwest China from local earthquake tomography. J. Volcanol. Geotherm. Res. 239, 83–91.
Xu, Z.Q., Wang, Q., Cai, Z.H., Dong, H.W., Li, H.Q., Chen, X.J., Duan, X.D., Cao, H., Li, J., Burg, J.P., 2015. Kinematics of the Tengchong Terrane in SE Tibet from the late Eocene to early Miocene: Insights from coeval mid-crustal detachments and strike-slip shear zones. Tectonophysics 665, 127–148.
Yang, H.Y., Hu, J.F., Hu, Y.L., Duan, Y.Z., Li, G.Q., 2013. Crustal structure in the Tengchong volcanic area and position of the magma chambers. J. Asian. Earth. Sci. 73, 48–56.
Yang, S.Q., Zhong, H., Zhu, W.G., Hu, W.J., Bai, Z.J., 2017. Platinum-group element geochemistry of mafic rocks from the Dongchuan area, southwestern China. Acta. Geochim. 36, 52–65.
Yin, A., Harrison, T.M., 2000. Geologic evolution of the Himalayan-Tibetan orogen. Ann. Rev. Earth. Plan. Sci. 28, 211–280.
Yin, G.M., Li, S.H., 2000. The thermoluminescence dating of the last eruption of Tengchong volcano (in chinese with English abstract). Earthq. Res. 23, 12–17.
Yu, H.m., Xu, J.D., Lin, C.Y., Shi, L.B., Chen, X.D., 2012. Magmatic processes inferred from chemical composition, texture and crystal size distribution of the Heikongshan lavas in the Tengchong volcanic field, SW China. J. Asian. Earth. Sci. 58, 1–15.
Zhao, C.P., Ran, H., Wang, Y., 2012. Present-day mantle-derived helium release in the Tengchong volcanic field, Southwest China: Implications for tectonics and magmatism (in chinese with English abstract). Acta Petrologica Sinica 28, 1189–1204.
Zhao, D.P., Yu, S., Ohtani, E., 2011. East Asia: seismotectonics, magmatism and mantle dynamics. J. Asian. Earth. Sci. 40, 689–709.
Zhao, Z.D., Mo, X.X., Dilek, Y., Niu, Y.L., Depaolo, D.J., Robinson, P., Zhu, D.C., Sun, C.G., Dong, G.C., Zhou, S., Luo, Z.H., Hou, Z.Q., 2009. Geochemical and Sr–Nd–Pb–O isotopic compositions of the post-collisional ultrapotassic magmatism in SW Tibet: Petrogenesis and implications for India intra-continental subduction beneath southern Tibet. Lithos 113, 190–212.
Zhou, M.F., Robinson, P.T., Wang, C.Y., Zhao, J.H., Yan, D.P., Gao, J.F., Malpas, J., 2012. Heterogeneous mantle source and magma differentiation of quaternary arc-like volcanic rocks from Tengchong, SE margin of the Tibetan Plateau. Contrib. Mineral. Petrol. 163, 841–860.
Zhu, B.Q., Mao, C.X., Lugmair, G.W., Macdougall, J.D., 1983. Isotopic and geochemical evidence for the origin of Plio-Pleistocene volcanic rocks near the Indo-Eurasian collisional margin at Tengchong, China. Earth. Planet. Sci. Lett. 65, 263–275.
Zou, H.B., Fan, Q.C., Schmitt, A.K., Sui, J.L., 2010. U-Th dating of zircons from Holocene potassic andesites (Maanshan volcano, Tengchon, SE Tibetan Plateau) by depth profiling: Time scales and nature of magma storage. Lithos 118, 202–210.
Zou, H.B., Ma, M.J., Fan, Q.C., Xu, B., Li, S.Q., Zhao, Y.W., King, D.T., 2017. Genesis and open-system evolution of Quaternary magmas beneath southeastern margin of Tibet: Constraints from Sr-Nd-Pb-Hf isotope systematics. Lithos 278–290.
Zou, H.B., Shen, C.C., Fan, Q.C., Lin, K., 2014. U-series disequilibrium in young Tengchong volcanics: Recycling of mature clay sediments or mudstones into the SE Tibetan mantle. Lithos 192–195, 132–141.